Acta Biochim Biophys Sin 2026, 58(7): 1637–1652
https://cstr.cn/32197.14.abbs.2025206
https://doi.org/10.3724/abbs.2025206
Original Article

Original Article

Total flavonoids of litchi seed attenuates cellular senescence by inhibiting the production of SASP through p65 suppression and ameliorates pulmonary fibrosis

Xiaocui Li[1,2,3,8,†,*], Yao Wei[1,†], Qiuchen Cheng[6,†], Suyu Xiao[5], Sisi Yao[5], Daikang Yang[1], Jilong Wang[5], Liping Chen[7], Qing Li[1,3,4,*], and Tingzheng Zhan[3,4,5,*]

[1]Department of Cell Biology and Genetics, School of Pre-clinical Medicine, Guangxi Medical University, Nanning 530021, China, [2]Education Department of Guangxi Zhuang Autonomous Region, Key Laboratory of Biological Molecular Medicine Research (Guangxi Medical University), Nanning 530021, China, [3]Key Laboratory of Longevity and Aging-Related Diseases of Chinese Ministry of Education, Guangxi Medical University, Nanning 530021, China, [4]Key Laboratory of Basic Research on Regional Diseases (Guangxi Medical University), Education Department of Guangxi Zhuang Autonomous Region, Nanning 530021, China, [5]Department of Parasitology, School of Pre-clinical Medicine, Guangxi Medical University, Nanning 530021, China, [6]Department of Gastroenterology, Institute of Digestive Disease, Guangxi Academy of Medical Sciences, the People's Hospital of Guangxi Zhuang Autonomous Region, Nanning 530021, China, [7]the Center for Medical Research, the Fifth Affiliated Hospital of Guangxi Medical University, Nanning 530022, China, and [8]Key Laboratory of Regenerative Medicine of Ministry of Education, Jinan University, Guangzhou 510632, China

[†]These authors contributed equally to this work.

*Correspondence address. E-mail: 222006@sr.gxmu.edu.cn (X.L.); qing_napier@126.com (Q.L.); ztznn@163.com (T.Z.)

Received 6 August 2025 Accepted 13 October 2025 Published 5 February 2026

Abstract

Anti-aging foods not only benefit elderly individuals but also drive the development of safe and effective natural drugs. Here, we report that the addition of total flavonoids of litchi seed (TFL) delays replicative senescence and stress-induced senescence. TFL alleviates the senescence-associated secretory phenotype (SASP) and reduces the degree of DNA damage caused by bleomycin (BLM). TFL also counteracts stress-induced pulmonary senescence and fibrosis. TFL reduces the protein level of p21 in mouse lung and alleviates pulmonary fibrosis. Transcriptome profiling further reveals that TFL plays a key role in its anti-aging mechanism by inhibiting the SASP. Mechanistically, TFL suppresses p65 protein expression, thereby inhibiting IL-1α and IL-1β and delaying cellular senescence. Gut microbiome analysis reveals that the abundance and functions of the mouse gut microbiome change after BLM exposure and that TFL treatment reverses these changes. Overall, we provide a theoretical basis for the future application of TFL as a potential anti-aging product.

Key words TFL, SASP, p65, senescence, IPF

Introduction

Aging is a complex biological process involved in the development of various diseases, including cancer [1], cardiovascular diseases [2], Alzheimer's disease [3], idiopathic pulmonary fibrosis [4], and type 2 diabetes [5]. In modern society, with the increasing elderly population, the burden on healthcare systems and economic resources continues to grow [6]. Therefore, preventing and managing age-related chronic diseases, as well as improving the health and quality of life of elderly individuals, holds significant social importance. Research on aging can be traced back to cellular senescence mechanisms. Cellular senescence manifests as cell cycle arrest, increased activity of β-galactosidase, heightened DNA damage signals, and elevated p21 and p16 protein levels, along with an increase in the senescence-associated secretory phenotype (SASP) [7,8]. These changes are crucial cellular responses to various internal and external stressors, such as DNA damage, telomere shortening, and mitochondrial dysfunctions [9,10].

In 2025, Kroemer *et al.* [11] identified fourteen key hallmarks of aging, including genomic instability, telomere attrition, epigenetic alterations, loss of proteostasis, disabled macroautophagy, deregu-

© The Author(s) 2025. This is an open access article distributed under the terms of the Creative Commons Attribution-NonCommercial-NoDerivs License (https://creativecommons.org/licenses/by-nc-nd/4.0/).

lated nutrient sensing, mitochondrial dysfunction, cellular senescence, stem cell exhaustion, extracellular matrix changes, altered intercellular communication, chronic inflammation, metabolic deregulation, and psychosocial isolation. Among these, the study of cellular senescence occupies a central position in understanding the mechanisms underlying aging. Cellular senescence promotes the secretion of SASP components, which release pro-inflammatory and pro-fibrotic factors that drive the initiation and progression of pulmonary fibrosis [12].

Idiopathic pulmonary fibrosis (IPF) is a relatively progressive interstitial lung disorder that leads to irreversible lung damage and ultimately death [13]. Currently, there is no effective pharmacological treatment for IPF due to an incomplete understanding of the fundamental cellular and molecular mechanisms [14,15]. IPF predominantly affects middle-aged and elderly populations and is correlated with increased mortality. Aging has been consistently identified as a significant risk determinant for IPF and is potentially linked to telomere shortening, mitochondrial dysfunction, and cellular senescence associated with the aging process [16,17].

Studies have indicated a close connection between cellular senescence and the development of IPF and that elevated levels of IL-1α/IL-1β resulting from DNA damage or telomere dysfunction promote disease progression [18,19]. In bleomycin-induced pulmonary fibrosis mouse models, IL-1α and IL-1β exert critical pro-inflammatory and pro-fibrotic effects by activating the NF-κB signaling pathway and stimulating myofibroblast differentiation, thereby driving the progression of fibrosis [18,19].

Anti-aging therapeutic approaches can be broadly categorized into two types: senolytic therapies that target the clearance of senescent cells (SnCs) and senomorphic strategies that aim to suppress the SASP [20–22]. Both approaches hold significant promise as potential interventions for modulating aging processes and treating age-related diseases.

Increasing evidence suggests that safe and effective drugs, particularly those targeting complex diseases, typically exert their therapeutic effects by modulating multiple molecular pathways rather than acting on one target [23,24]. Natural products have constituted the cornerstone of disease prevention and treatment strategies for millennia, embodying rich traditional wisdom and serving as valuable resources for drug discovery [25].

Chinese herbal medicine (CHM) exhibits distinct multi-component and multi-target characteristics [26,27]. The multi-targeting phytochemical ensembles of CHM show greater efficacy than single agents against complex diseases, including age-related pathologies [28–30]. Owing to their proven safety profile and effectiveness, herbal formulations are increasingly favored in the development of combination therapies [31,32].

Lychee is a key economic plant in southern China. The region boasts a rich diversity of lychee germplasm resources and benefits from exceptional geographical advantages. The total flavonoids of litchi seed (TFL) are rich in compounds such as rutin and quercetin, which have demonstrated notable potential in areas such as antioxidation and cancer prevention [33,34]. Previous studies have indicated that TFL can alleviate schistosomiasis-induced liver fibrosis by inhibiting hepatic stellate cell activation and modulating the gut microbiota [35]. TFL has also been shown to be effective in treating CCl_4-induced liver fibrosis, as well as in conditions such as alcoholic fatty liver disease and cirrhosis [36]. Like liver fibrosis, pulmonary fibrosis shares many markers, such as inflammatory factors, with aging. However, whether TFL also possesses anti-aging effects remains unknown.

In the present study, we established aging models in both cells and mice and treated them with TFL. We observed morphological changes in cells and tissues, and by detecting the expression of senescence markers in cell and mouse tissue samples, we found that TFL reduced the percentage of SA-β-Gal-positive cells and decreased p21 protein expression by inhibiting the release of inflammatory factors such as IL-1α and IL-1β. Through RNA sequencing, we identified NF-κB signaling as one of the key targets of TFL. Specifically, TFL suppresses the expression of p65 to decrease the release of SASP components, thereby delaying aging. Analysis of the gut microbiome revealed that bleomycin (BLM) exposure altered the abundance and functional profiles of the gut microbiota in mice, which were subsequently restored by TFL treatment. Overall, our findings suggest that TFL can delay the aging process by inhibiting p65-driven SASP secretion, highlighting its potential as an anti-aging therapeutic agent.

Materials and Methods

Cell culture and transfection

MRC-5 human lung fibroblast cells were acquired from the Cell Resource Center at Peking Union Medical College (Beijing, China). Cells were cultured in DMEM (GIBCO, Carlsbad, USA) supplemented with 10% FBS (GIBCO) and antibiotic-antimycotic solution (penicillin-streptomycin, 100 U/mL; GIBCO) under standard conditions (37°C, 5% CO_2). Plasmid DNA was transiently transfected into MRC-5 fibroblasts via Lipofectamine RNAiMAX (Thermo Fisher Scientific, Waltham, USA) following the manufacturer's protocol. Briefly, cells were seeded in 6-well plates, transfected with 1–2 μg of plasmid DNA using Lipofectamine RNAiMAX, and harvested 72 h post-transfection for analysis. The pcDNA3.1-HA-p65 was obtained from Dr. Liu Kunpeng's laboratory at Guangxi University (Nanning, China). The pcDNA3.1-HA was empty vector from Dr. Li Xiaocui's laboratory at Guangxi Medical University.

Cell treatments

Cells were simultaneously treated with VP-16 (2 μM; Thermo Fisher Scientific) or BLM (10 μM; Selleck, Houston, USA) and either low-dose TFL (TFL-L; 300 mg/L) or high-dose TFL (TFL-H; 450 mg/L). VP-16 or BLM treatment was maintained for 4 days, whereas TFL treatment was continued for a total of 6 days. TFL (ZC16081016) was purchased from Herb Source Biotechnology (Nanjing, China), and the chemical composition of TFL was analyzed at the Center of Pharmaceutical Technology at Tsinghua University (Beijing, China). Its extraction and purification methods, composition and relative abundance have been described previously [35–37]. The general procedure involves: washing and drying litchi seeds, grinding and sieving through a 20-mesh sieve, ethanol reflux extraction (500 mL/L), collection of total extract paste, water dissolution, passage through D-101 macroporous resin (Baoen, Cangzhou, China), ethanol elution (800 mL/L), rotary evaporation of the eluate, additional ethanol reflux followed by filtration, repeated rotary evaporation, and drying to obtain TFL powder. The total flavonoid content is 835 g/kg, as determined by HPLC (Herb Source Biotechnology).

Gene silencing

siRNAs were transfected into target cells via Lipofectamine RNAi-

MAX according to the manufacturer's instructions. siRNAs (p65: 5′-GCCCUAUCCCUUUACGUCAdTdT-3′) were purchased from Sangon Biotech (Shanghai, China). A scrambled sequence (NC: 5′-UUCUCC GAACGUGUCACGUdTdT-3′) served as a control.

Western blot analysis

Western blot assays were performed according to standard protocols. The antibodies used were as follows: γH2AX (1:4000, ab26350; Abcam, Cambridge, UK), p16 (1:1000, 554079; BD Biosciences, San Jose, USA), p21 (1:1000, F0170; Selleck, Shanghai, China), p65 (1:1000, F0006; Selleck), GAPDH (1:5000, GB15002; Servivebio, Wuhan, China) and HRP-conjugated anti-rabbit or anti-mouse IgG secondary antibodies (KPL, Gaithersburg, USA).

Immunofluorescence (IF) staining

The cells on coverslips were fixed (4% paraformaldehyde, 15 min), permeabilized (0.2% Triton X-100, 10 min), and blocked (5% goat serum, 1 h). Coverslips were incubated with primary antibody (4°C, overnight) followed by incubation with a fluorescent secondary antibody (RT, 1 h). The cells were stained with DAPI and visualized via fluorescence microscopy. The following antibodies were used: anti-γH2AX antibody (1:400, ab26350; Abcam), DyLight488 (1:500, BA1126; BOSTER, Wuhan, China).

Experimental animals

Specific pathogen-free (SPF) female C57BL/6 mice, aged 6–8 weeks and weighing 18–20 g, were provided by the Animal Center of Guangxi Medical University (Nanning, China). Animal studies complied with China's Laboratory Animal Guidelines and were approved by Guangxi Medical University's Ethics Committee (No. 202412009). Mice were randomized into control (n = 5), BLM (n = 5), and BLM + TFL-H (450 mg/kg, n = 5) groups. Each mouse in the BLM and BLM + TFL-H groups was injected with BLM (2.5 mg/kg body weight). TFL solutions were prepared in pure water. TFL treatment (450 mg/kg, daily oral gavage) began at BLM induction and continued for 14 days. After the last treatment, the mice were euthanized with CO_2. Harvested lungs were weighed, with portions fixed in 4% PFA for histological examination or snap-frozen (–80°C) for downstream assays.

Analysis of the gut microbiome

Fecal samples from mice in the Control group, BLM group, and BLM + TFL group were submitted to Sangon Biotech for 16S rRNA analysis. The specific procedures were as follows:

For downstream microbiome profiling, genomic DNA was extracted from environmental samples using the E.Z.N.A™ Mag-Bind Soil DNA Kit (M5635-02; Omega, Norcross, USA) following the manufacturer's protocols. PCR amplification of the 16S rRNA gene was performed with the standard three-step thermal cycling. The PCR products were confirmed using 2% (w/v) agarose gel electrophoresis in TBE buffer, ethidium bromide staining, and UV visualization.

Purification of amplicons was performed with Hieff NGS™ DNA Selection Beads (10105ES03; Yeasen, Shanghai, China) to eliminate residual primers and primer dimers. Subsequent library preparation was carried out by Sangon Biotech employing standard Illumina adaptors and indices. Prior to sequencing, PCR amplicons were quantified using the Qubit® 4.0 Green dsDNA assay (Thermo Fisher Scientific), and assessed for quality on an Agilent 2100 Bioanalyzer (Agilent, Santa Clara, USA). Libraries were normalized to equimolar concentrations based on coverage requirements and sequenced on the Illumina MiSeq system (USA) following the manufacturer's protocol.

Illumina reads were assembled using PEAR software (v0.9.8) based on overlapping regions, and fastq files were processed into fasta and qual files. High-quality reads were clustered into operational taxonomic units (OTUs) at a 97% similarity cut off using Usearch software (v11.0.667). Chimeric sequences and singleton OTUs were filtered out, and remaining sequences were reassigned to their original samples according to OTU membership. The most abundant tag sequence within each OTU was designated as its representative. Bacterial and fungal representative OTU sequences were assigned taxonomy by conducting a BLAST search against the RDP and the UNITE ITS reference Database, respectively.

The α-diversity indices (including Simpson index) were quantified in terms of OTU richness. All α diversity indices were calculated with Mothur software (version 3.8.31). The OTU rank abundance curves (for microbial abundance analysis) were plotted in R-ggplot2. To estimate the diversity of the microbial community of the sample and conduct multiple group comparisons, we used Analysis of Variance (ANOVA) test in STAMP software (version 2.1.3) for assessing the significance of differences in mean values among two or more sample groups.

SA-β-Gal staining

SA-β-Gal staining was performed on MRC-5 cells and mouse lung tissues using a senescence β-galactosidase staining kit (C0602; Beyotime, Shanghai, China) following the manufacturer's instructions. MRC-5 cells and mouse lung tissues were fixed properly. Fixed MRC-5 cells were incubated with staining solution at 37°C overnight. Fixed mouse lung tissues were incubated with staining solution at 37°C for 48 h.

RNA extraction and qRT-PCR

Total RNA was extracted from MRC-5 cells and lung tissues via the TRIzol reagent (Invitrogen, Carlsbad, USA), and total cDNA was synthesized via the Takara PrimeScript RT reagent kit (Takara, Tokyo, Japan). The primers used are listed in Supplementary Table S1.

Immunohistochemical (IHC) analysis

IHC assays were performed according to standard protocols. The following antibodies were used: anti-α-SMA (1:2500, 80008-1-RR; Proteintech, Wuhan, China) and anti-p21 (1:1000, ab188224; Abcam). The fluorescent secondary antibody was used: Poly-HRP Goat Anti Rabbit Secondary Antibody (H + L) secondary antibody (HKI0026; HaoKebio, Hangzhou, China).

Histopathological analysis

Lung tissues were fixed in 4% PFA, paraffin-embedded, and sectioned (4 μm) for hematoxylin and eosin (H&E) staining (G1120; Solarbio). Histopathological images were analyzed to quantify lesion areas. The Ashcroft score was determined in a blinded manner in accordance with previous studies [38]. Collagen deposition (fibrosis indicator) was assessed via Masson's trichrome staining (G1340; Solarbio). The stained sections were also analyzed via ImageJ software to measure the collagen fiber area.

RNA sequencing

MRC-5 cells from the DMSO and TFL-H groups were collected for RNA sequencing analysis ($n = 3$). RNA purification, reverse transcription, library construction, and sequencing were performed by Beijing Tsingke Biotechnology Co., Ltd (Beijing, China) following the manufacturer's protocols (Illumina, San Diego, USA).

For RNA sequencing library preparation, the Illumina® Stranded mRNA Prep Ligation Kit was used, starting with 1 μg of total RNA. Poly(A)-containing mRNA was enriched via oligo(dT)-coupled magnetic beads, followed by fragmentation under optimized buffer conditions. First- and second-strand cDNA synthesis was performed via random hexamer primers (Illumina) and the SuperScript Double-Stranded cDNA Synthesis Kit (Invitrogen). Subsequent steps included end repair, phosphorylation, and 'A' tailing, following the manufacturer's standardized workflow.

The raw sequencing data were processed via SOAPnuke (v1.5.2) with the following quality control steps: removal of reads containing sequencing adapters; exclusion of reads with > 20% low-quality bases (quality score ≤ 5); and elimination of reads with > 5% unknown bases ('N'). The resulting high-quality clean reads were stored in FASTQ format and subsequently aligned to the reference genome via HISAT2 (v2.0.4). For gene expression quantification, clean reads were mapped to the reference coding gene set via Bowtie2 (v2.2.5), followed by expression level calculation via StringTie (v2.1.2). Differential expression analysis was conducted with DESeq2 (v1.4.5), applying a significance threshold of a Q value ≤ 0.05. To investigate phenotypic associations, KEGG pathway enrichment analysis of differentially expressed genes was performed via the hypergeometric test (Phyper). Significant terms (Q value ≤ 0.05, Bonferroni-corrected) were identified.

Statistical analysis

All the data are presented as the mean ± SEM. Statistical significance was determined by unpaired two-tailed *t* tests or one-way ANOVA. $P < 0.05$ indicated significant difference.

Results

TFL alleviates cellular senescence

To explore the anti-aging effect of TFL, PD35 MRC-5 cells were treated with different concentrations of TFL. After 6 days of treatment, 17.9% of the control MRC-5 cells were positively stained with SA-β-Gal. In cells treated with TFL, the percentage of SA-β-Gal-positive cells was reduced to 11.29% (TFL-L) and 9.14% (TFL-H) (Figure 1A,B). Since SA-β-Gal activity is an important indicator of cellular senescence, our results indicated that TFL exhibited an anti-aging effect in a concentration-dependent manner. We also detected a number of senescence markers in MRC-5 cells. Compared with those in control MRC-5 cells, the mRNA and protein levels of p21, the most well-known senescence marker, were significantly lower in the TFL-L and TFL-H groups (Figure 1C,D). Similarly, the mRNA and protein levels of p16 were also significantly reduced in the TFL-L and TFL-H groups in a concentration-dependent manner (Supplementary Figure S1A,B). The mRNA levels of IL-1α, IL-1β, and IL-6, three important inflammatory markers, were also significantly reduced in the TFL-L and TFL-H groups (Figure 1E). The mRNA levels of IL-8 and MMP2 were significantly reduced in the TFL-H group (Figure 1E).

We also replicated these experiments in PD45 presenescent MRC-5 cells and observed similar results. In cells treated with TFL, SA-β-Gal-positive cells were significantly reduced in both the TFL-L (33.81%) and TFL-H (32.49%) groups compared with the control (DMSO) group (42.29%) (Supplementary Figure S1C,D). The mRNA levels of IL-1α, IL-1β, and IL-6, as well as those of IL-8 and MMP2, were also significantly reduced in the TFL-H group (Supplementary Figure S1E). Taken together, these results indicated that TFL treatment downregulated the expression of senescence markers and delayed senescence in MRC-5 cells.

TFL alleviates stress-induced senescence in MRC-5 cells

We next investigated whether TFL is effective in alleviating stress-induced senescence in MRC-5 cells. When cells were treated with both BLM and different concentrations of TFL, we observed a significant attenuation of cellular senescence phenotypes following TFL administration. In the BLM group, the percentage of SA-β-Gal-positive cells was 47.39%. In the BLM + TFL groups, the percentage of SA-β-Gal-positive cells significantly decreased to 35.32% (TFL-L) and 26.83% (TFL-H) (Figure 2A,B), indicating a concentration-dependent anti-aging effect of TFL. Similarly, the mRNA and protein levels of p21 were also significantly lower in the BLM + TFL groups (Figure 2C,D). Compared with the p16, IL-1α, IL-1β, IL-6, IL-8, and MMP2 mRNA levels in the BLM group, the mRNA levels in the BLM + TFL groups were also significantly lower (Figure 2E,F).

We also tested the anti-senescence effect of TFL by using a different agent, VP-16, to induce senescence in MRC-5 cells, and we observed similar results as those in the VP-16-induced MRC-5 cell senescence model. When cells were treated with VP-16 and different concentrations of TFL, we observed a significant attenuation of cellular senescence phenotypes following TFL administration. In the VP-16 group, the percentage of SA-β-Gal-positive cells was 17.22%. In the VP-16 + TFL groups, the percentage of SA-β-Gal-positive cells significantly decreased to 9.17% (TFL-L) and 8.85% (TFL-H) (Supplementary Figure S2A,B). Similarly, the protein levels of p21 and p16 were also significantly reduced in the VP-16 + TFL groups (Supplementary Figure S2C,D). We also found that the mRNA levels of p21 and p16 decreased after TFL treatment (Supplementary Figure S2E). Taken together, these results indicated that TFL alleviated both BLM- and VP16-induced senescence in MRC-5 cells.

TFL alleviates the DNA damage response

We next explored whether TFL can protect cells from DNA damage-induced senescence. As an important DNA damage marker, the γH2AX protein levels in both presenescent MRC-5 cells and BLM-induced senescent cells were detected by western blot analysis. In presenescent MRC-5 cells, TFL treatment significantly reduced γH2AX protein expression in a concentration-dependent manner (Figure 3A). BLM triggers senescence by inducing DNA double-strand breaks that activate damage response pathways, ultimately leading to cell cycle exit [39]. The protein level of γH2AX increased in the BLM group, but this spike was significantly reduced in the BLM + TFL groups (Figure 3B). Immunofluorescence detection of the γH2AX signal also revealed results similar to those of the western blot analysis. After 10 μM BLM treatment, the fluorescence signal of γH2AX in the BLM group significantly increased, suggesting a robust DNA damage signal. Compared with that in the BLM + TFL group, the average number of γH2AX foci in the BLM group was significantly decreased in a concentration-dependent

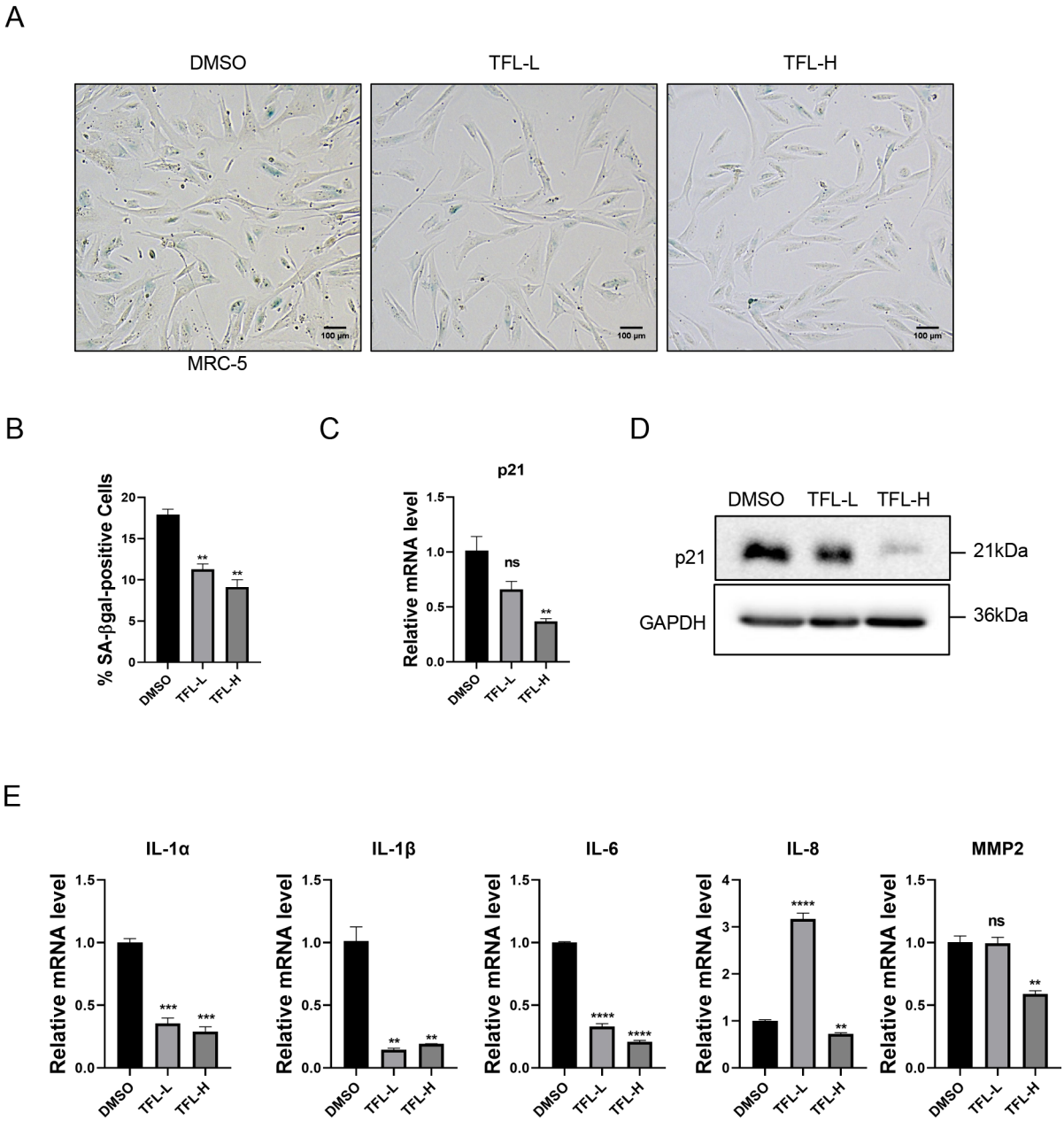

Figure 1. TFL alleviates cellular senescence (A) SA-β-Gal staining of PD35 MRC-5 cells treated with 300 mg/L (TFL-L) or 450 mg/L (TFL-H) TFL for 6 d. Scale bar: 100 μm. (B) Quantification of (A). The percentage of SA-β-Gal-positive cells was calculated ($n \geq 100$ cells). (C) mRNA levels of *p21* after TFL treatment for 6 d. (D) Protein levels of p21 after TFL treatment for 6 d. (E) mRNA levels of senescence-associated secreted protein (SASP) genes after TFL treatment for 6 d. Data are presented as the mean ± SEM. Statistical significance was assessed via two-tailed unpaired Student's *t* tests (*$P < 0.05$, **$P < 0.01$, ***$P < 0.001$, ****$P < 0.0001$). See also Supplementary Figure S1.

manner, indicating that TFL treatment reduced the extent of DNA damage (Figure 3C,D).

TFL alleviates BLM-induced senescence in mice

We next explored whether TFL is effective in alleviating BLM-induced lung fibrosis and senescence in mice (Figure 4A). To establish a pulmonary fibrosis model, we administered BLM via intratracheal instillation in mice, a well-characterized approach that mimics the key pathological features of IPF in humans [40]. SA-β-Gal staining of the mouse lung tissue revealed that, in the control (saline) groups, the lung samples were not stained and remained the original color; in the BLM group, most of the lung samples were heavily stained by SA-β-Gal and displayed a strong blue color; and in the TFL-H group, the positively stained areas of the lung samples were much smaller than those in the BLM group (Figure 4B). The mRNA levels of IL-1α, IL-1β, IL-6, and TGF-β, four important inflammatory markers, were also significantly reduced in the TFL-H group (Figure 4C). The mRNA and protein levels of p21 were also significantly lower in the TFL-H group than in the BLM group (Figure 4D–F and Supplementary Figure S3A), which is consistent

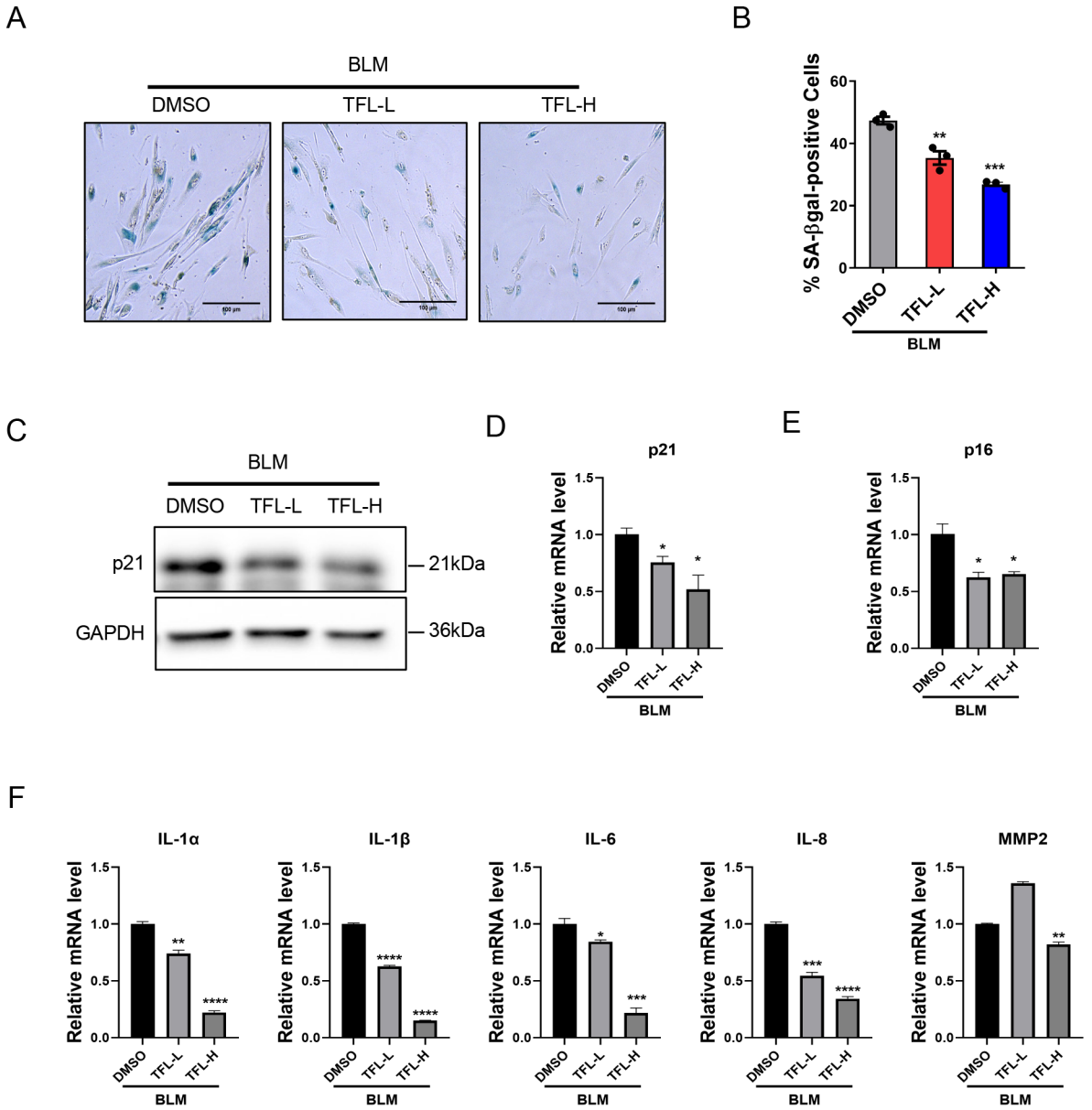

Figure 2. TFL alleviates BLM-induced senescence (A) SA-β-Gal staining of MRC-5 cells treated with BLM and TFL. Cells were treated with 10 μM BLM for 4 d, and 300 mg/L (TFL-L) or 450 mg/L (TFL-H) TFL was added to the BLM-treated cells for 6 d at the same time. Scale bar: 100 μm. (B) Quantification of A. The percentage of SA-β-Gal-positive cells was calculated ($n \geq 100$ cells). (C) Protein levels of p21. (D) mRNA levels of *p21*. (E) mRNA levels of *p16*. (F) mRNA levels of *SASP* genes. Data are presented as the mean ± SEM. Statistical significance was assessed via two-tailed unpaired Student's *t* tests (*$P < 0.05$, **$P < 0.01$, ***$P < 0.001$, ****$P < 0.0001$). See also Supplementary Figure S2.

with the results shown in Figure 2 that TFL alleviated BLM-induced cell senescence. We detected reduced p21 protein levels in the lung tissue via IHC analysis (Figure 4G,H). The IHC results revealed a statistically significant increase in p21 expression in BLM-treated tissues, as evidenced by extensive brown-yellow staining. In contrast, the BLM + TFL-H treatment group presented a significant reduction in positive expression (Figure 4G). ImageJ analysis revealed that p21 expression was significantly elevated in the BLM group and significantly decreased after TFL treatment (Figure 4H). Taken together, these results indicated that TFL reduced the expression of senescence markers and alleviated BLM-induced senescence in mice.

TFL improves BLM-induced pulmonary fibrosis

Fibrosis progression was assessed via combined α-SMA immunohistochemistry (IHC) (activation marker), H&E (histological injury), and Masson's trichrome (collagen deposition) analyses. Masson's trichrome staining revealed high-density collagen staining and marked proliferation of collagen fibers in the BLM group. TFL treatment markedly attenuated pulmonary fibrotic progression, as evidenced by significantly reduced collagen deposition (Figure 5A, B). IHC results revealed that the expression of α-SMA, the most

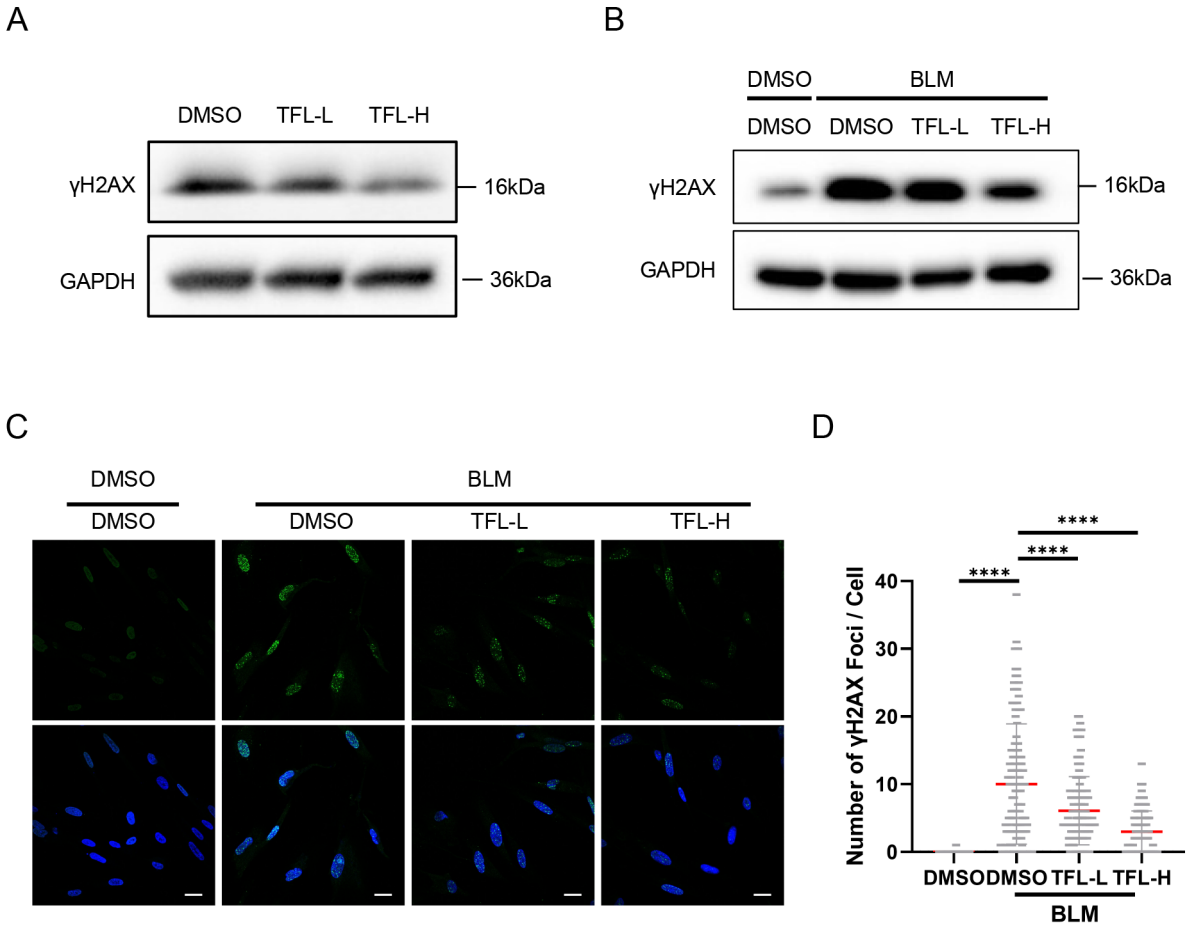

Figure 3. TFL alleviates DNA damage (A) Protein levels of γH2AX in presenescent MRC-5 cells after 6 days of 300 mg/L (TFL-L) or 450 mg/L (TFL-H) TFL treatment. (B) Protein levels of γH2AX in PD32 MRC-5 cells treated with BLM and TFL. Cells were treated with 10 μM BLM for 4 d, and TFL was added to the BLM-treated cells for 6 d at the same time. (C) Immunofluorescence analysis of γH2AX in MRC-5 cells treated with 10 μM BLM or TFL for 4 d. Scale bar: 20 μm. (D) The number of γH2AX foci was statistically analyzed ($n \geq 100$ cells). Data are presented as the mean ± SEM. Statistical significance was assessed via two-tailed unpaired Student's *t* tests (*$P < 0.05$, **$P < 0.01$, ***$P < 0.001$, ****$P < 0.0001$).

important fibrosis marker, was significantly increased in the BLM group. In contrast, in the TFL-H group, brown-yellow staining was lighter, and the area was smaller, indicating a significant reduction in α-SMA expression (Figure 5C,D). H&E staining revealed that BLM treatment partially disrupted the alveolar structure of the lung tissue, with widened alveolar septa and increased density, but the aforementioned detrimental pathological changes were ameliorated after TFL treatment (Figure 5E). Blinded histological analysis via the Ashcroft score revealed markedly less lung fibrosis in the TFL-treated mice than in the BLM-treated mice (Figure 5F). Taken together, these results indicated that BLM-induced pulmonary senescence and fibrosis were significantly ameliorated by TFL treatment.

Key pathways involved in the anti-aging mechanism of TFL

To further study the key genes and pathways involved in the anti-aging mechanism of TFL, we performed RNA sequencing in MRC-5 cells treated with DMSO or TFL for 6 days (Figure 6A). Three independent replicate samples for both the DMSO group and TFL group were sequenced. The 1218 downregulated genes included *IL-1α*, *IL-1β*, *IL-11*, *IL-24*, *CCL2*, *MMP1*, and *TGF-β* (Figure 6A,B), strongly suggesting that TFL suppresses the release of SASP components, which is consistent with the data shown in Figure 1E. Gene set enrichment analysis (GSEA) revealed significant negative enrichment of the cellular senescence pathway in TFL-treated cells (Figure 6C), further supporting the anti-aging effect of TFL at the transcriptomic level. GSEA of the DEGs in TFL-treated cells revealed that these genes are also involved in the NF-κB signaling pathway (Supplementary Figure S4). Moreover, transcriptome sequencing revealed that many pathways, including the PI3K-AKT, cytokine–cytokine receptor interaction and NF-κB signaling pathways, changed in response to TFL treatment according to KEGG analysis (Figure 6D). A KEGG pathway plot further revealed that TFL may inhibit SASP release by targeting NF-κB (Figure 6E), as NF-κB is the main protein that regulates SASP transcription [8]. On the other hand, transcriptome sequencing revealed metabolic changes in response to TFL treatment (Figure 6F). KEGG enrichment of the differentially abundant metabolites in TFL-treated cells revealed "carbon metabolism", "biosynthesis of amino acids", and "vitamin B6 metabolism" (Figure 6F). Collectively, these results demonstrated that TFL exerts its rejuvenating

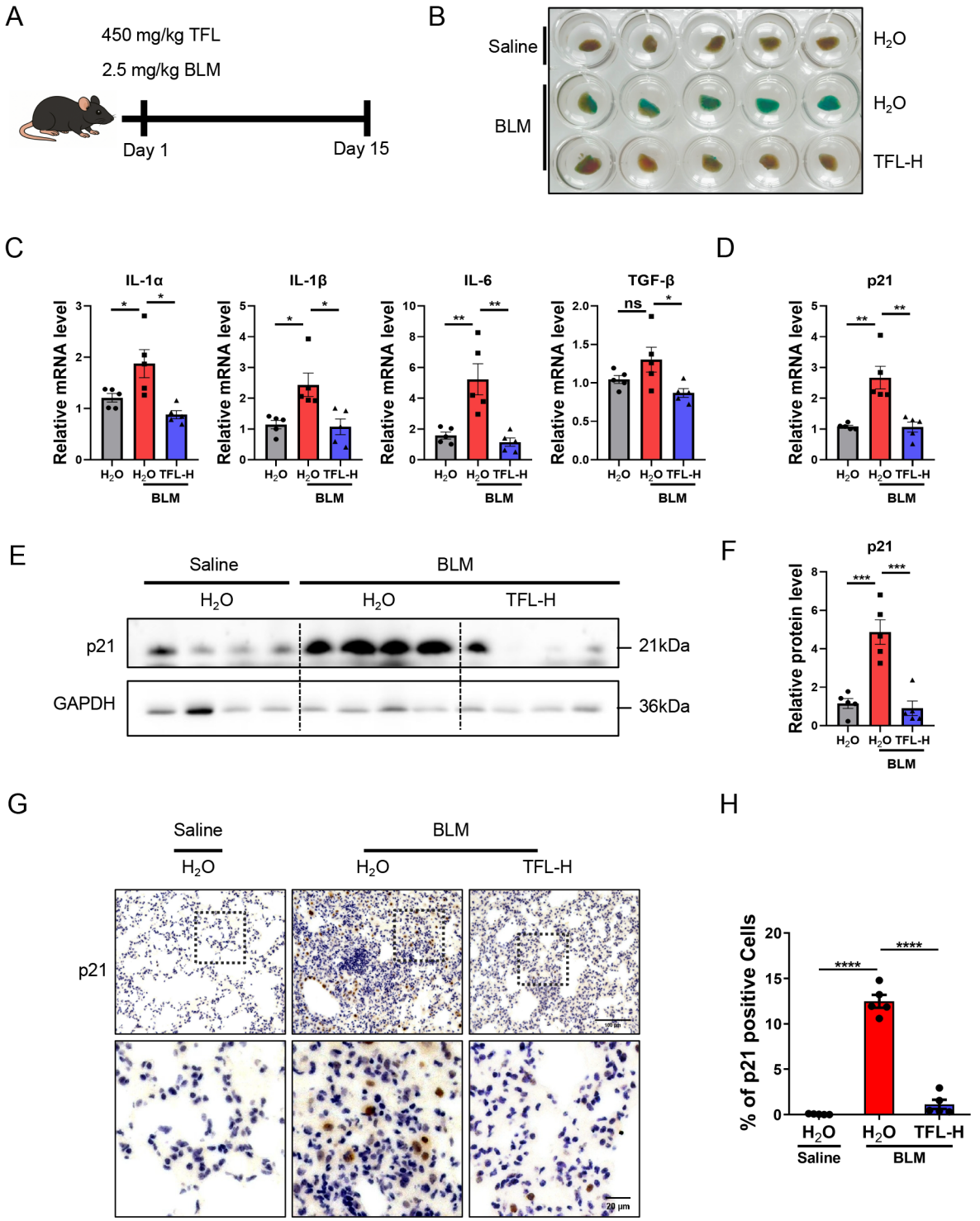

Figure 4. TFL alleviates BLM-induced pulmonary senescence (A) Schematic diagram of mouse IPF model construction and TFL treatment. (B) SA-β-Gal staining of mouse lung samples. Senescent cells decreased in IPF mouse lungs after 450 mg/L (TFL-H) TFL treatment. (C) SASP factors in mouse lungs from panel A were detected via RT-qPCR (n = 5 per group). (D) mRNA levels of *p16* and *p21* in mouse lungs from panel A were detected via RT-qPCR (n = 5). (E) The protein level of p21 in the lungs of the mice in panel A was detected via western blotting. (F) Quantification of (E) and Supplementary Figure S3A. The intensity of p21 was calculated (n = 5). (G) p21 protein in lungs from panel A was detected by IHC. (H) Quantification of the data in G. Data are presented as the mean ± SEM of 5 mice. Statistical significance was assessed via two-tailed unpaired Student's t tests (*P < 0.05, **P < 0.01, ***P < 0.001, ****P < 0.0001). See also Supplementary Figure S3.

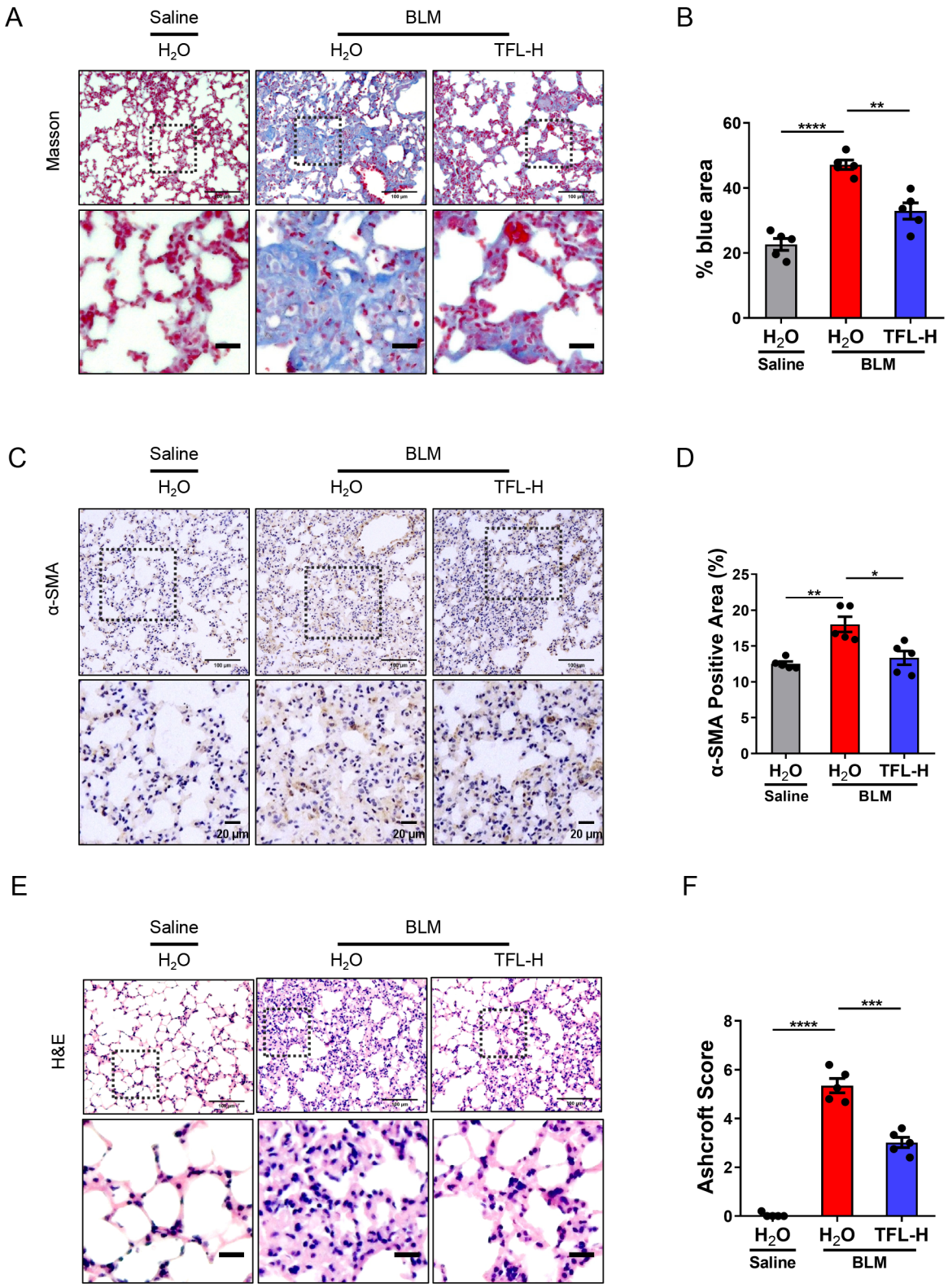

Figure 5. TFL improves BLM-induced pulmonary fibrosis (A) Masson's trichrome staining of mouse lungs. Scale bar: 100 μm (top), 20 μm (bottom). (B) Percentage of collagen area (blue) from (A). (C) IHC staining of the α-SMA protein in mouse lungs. (D) The percentage of the α-SMA-positive area in (C). (E) H&E staining of mouse lungs. Scale bar: 100 μm (top), 20 μm (bottom). (F) Ashcroft scores of mouse lung fibrosis samples from (E). Data are presented as the mean ± SEM. Statistical significance was assessed via two-tailed unpaired Student's *t* tests (**P* < 0.05, ***P* < 0.01, ****P* < 0.001, *****P* < 0.0001).

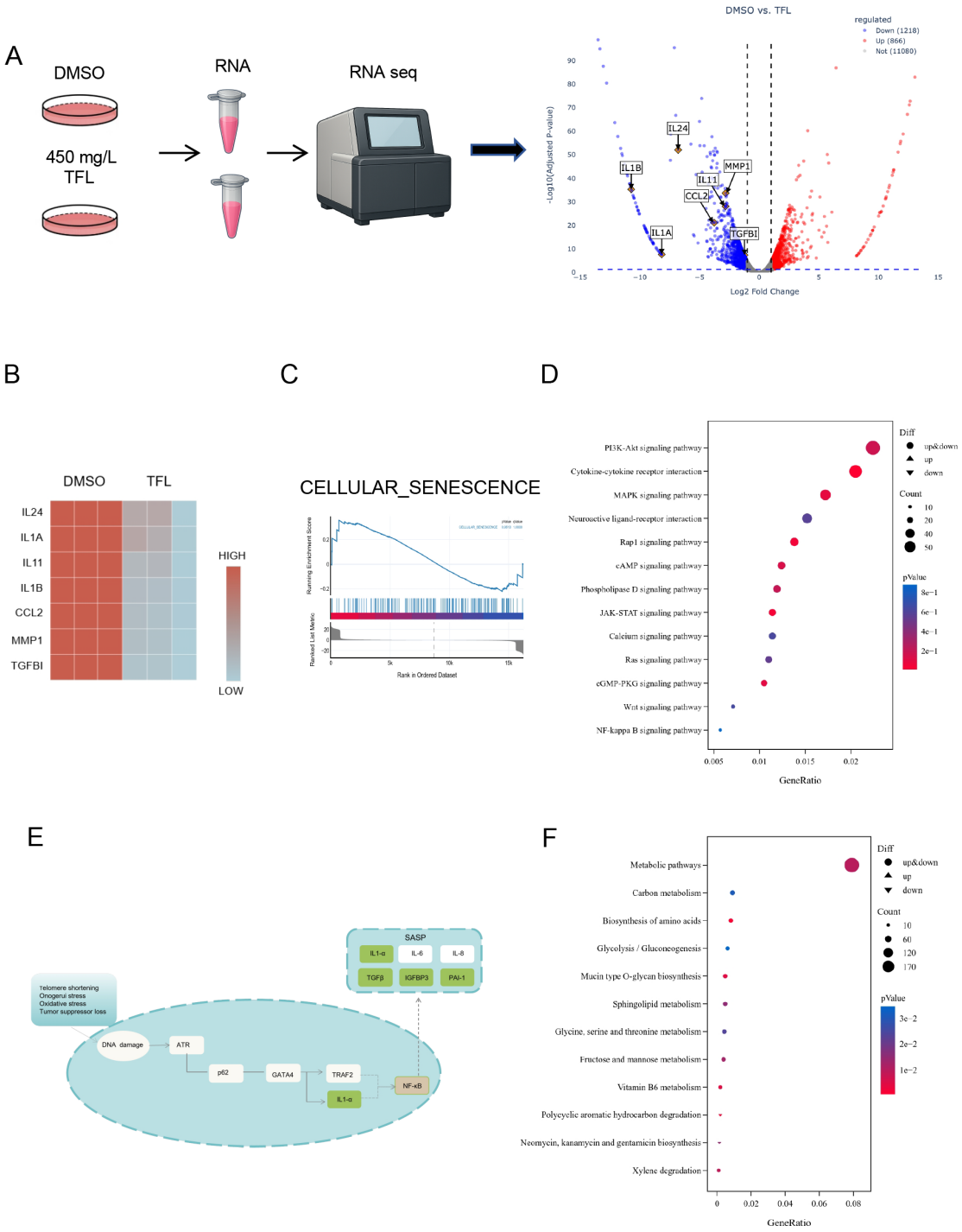

Figure 6. TFL targets multiple pathways and metabolically modulates rejuvenation (A) Schematic representation of TFL and age-related gene collection. Volcano plot of differentially abundant RNAs in TFL-treated cells. (B) Heatmap visualization of the inflammatory factors involved in senescence from (A). (C) GSEA of DEGs in TFL-treated cells showing cellular senescence. (D) KEGG dot plot of differentially expressed genes involved in environmental information processes in TFL-treated cells. (E) A KEGG pathway plot was generated to show SASP regulation in the cellular senescence pathway. Green: protein downregulation. (F) KEGG dot plot of DEGs involved in metabolic processes in TFL-treated cells. See also Supplementary Figure S4.

effects by targeting the NF-κB signaling pathway, repressing SASP-related gene expression, and altering metabolic pathways, highlighting its potential as a therapeutic agent for mitigating cellular senescence.

TFL alleviates senescence via the inhibition of p65 in the NF-κB signaling pathway

To further explore the anti-aging mechanism and identify the targets of TFL, we determined the mRNA and protein levels of key

genes selected from our RNA sequencing results. p65 is the main subunit of the NF-κB signaling pathway in cellular senescence, which regulates the release of SASP factors, such as IL-1α and IL-1β [8,41,42]. In PD35 MRC-5 cells, the mRNA level of p65 was significantly reduced after high-dose TFL treatment, and the p65 protein level was significantly reduced after both high- and low-dose TFL treatment (Figure 7A,B). In BLM-induced senescent MRC-5 cells, the protein level of p65 was also significantly decreased after TFL treatment (Figure 7C), indicating that TFL delayed cellular senescence by inhibiting p65 protein expression. To further confirm that p65 is a target of TFL, a rescue experiment was conducted via the transfection of a p65 plasmid into TFL-treated MRC-5 cells. Compared with the control (DMSO) treatment, TFL treatment significantly reduced the proportion of SA-β-Gal-positive cells (Figure 7D–E). However, in the TFL+p65 group, the proportion of SA-β-Gal-positive cells was partially restored compared with that in the TFL + EV (empty vector) group, indicating that p65 overexpression partially reversed the anti-aging effect of TFL (Figure 7D–E). To further validate this finding, we examined the protein level of p21 via western blot analysis. TFL treatment reduced the expression of p21, whereas p65 overexpression reversed this effect, leading to increased p21 levels (Figure 7F). Additionally, TFL significantly suppressed the mRNA levels of *IL-1α* and *IL-1β*, which were partially restored by p65 overexpression (Figure 7G). These results collectively demonstrated that TFL alleviates senescence-associated phenotypes by decreasing p65 protein levels. To further confirm that TFL delays senescence via p65 inhibition, we knocked down *p65* via siRNA and observed significant downregulation of p21, SA-β-Gal, IL-1α, and IL-1β, which was consistent with the effects of TFL treatment (Figure 7H,I, and Supplementary Figure S5A,B). When siRNA and TFL were applied simultaneously, no additive inhibitory effect was observed on p21, SA-β-Gal, IL-1α, or IL-1β compared with the effects of the individual treatments (Figure 7H,I and Supplementary Figure S5A,B), suggesting that TFL and *p65* knockdown act through the same signaling pathway.

TFL treatment improves the changes in the gut microbiome caused by BLM

Analysis of the gut microbiome in mouse fecal samples revealed that the Simpson index of the species decreased after BLM treatment. The index exhibited recovery after TFL treatment, although this improvement did not reach statistical significance (Figure 8A). The number of species in the three groups (799, 856, and 809) did not significantly differ (Supplementary Figure S6). Among them, the relative abundances of *norank_Lachnospiraceae* and *Alistipes* exhibited a “low-high-low” trend across the control group, the BLM group, and the BLM + TFL-H group, respectively (Figure 8B,C). Conversely, *norank_Muribaculaceae*, *Lactobacillus*, and *norank_Prevotellaceae* displayed a “high-low-high” trend (Figure 8B,C). *norank_Muribaculaceae* and *Lactobacillus* are common beneficial bacteria [43,44] whose abundance decreases after BLM treatment but recovers following TFL intervention. While Alistipes has been shown to aggravate colorectal cancer [45,46], its role in pulmonary fibrosis has rarely been explored. We found that the abundance of Alistipes increased following BLM treatment but subsequently recovered upon TFL intervention (Figure 8B,C). Taken together, these results indicated that TFL treatment ameliorated the BLM-induced alterations in gut microbiome species richness and increased the relative abundance of beneficial bacteria.

Discussion

Aging and health represent complex scientific issues regulated by multidimensional factors. Advances in modern medicine have significantly extended the average lifespan, but this has resulted in an aging population with a rising incidence of age-related chronic diseases such as Alzheimer’s disease, atherosclerotic cardiovascular disease, and type 2 diabetes. Consequently, researchers are increasingly focusing on developing safe, effective anti-aging interventions, particularly small-molecule drugs and natural products.

Owing to their abundance of bioactive compounds and characteristic multi-component, multi-target, and synergistic therapeutic properties, natural products have unique advantages in disease prevention, particularly in aging intervention. TFL is a group of bioactive components extracted from litchi seeds that are widely distributed in southern China. Its safety has long been tested in the context of traditional Chinese medicine practices. A previous study by Wan *et al.* [47] showed that even at the maximum oral dosage, TFL did not exhibit toxicity in mice. These results demonstrate that the use of TFL is safe. TFL has been shown to effectively alleviate liver fibrosis induced by CCl_4. This protective effect may be mediated through the upregulation of the retinoic acid metabolism pathway, which influences lipid metabolism and extracellular matrix degradation [36]. Additionally, TFL could effectively attenuate the self-renewal capacity of breast cancer stem cells by significantly downregulating the expression levels of core stemness transcription factors (Oct4, Nanog, *etc.*), thereby suppressing their tumor-initiating potential [33].

Our earlier work revealed that TFL can improve liver fibrosis in mice infected with *Schistosoma japonicum* [35]. The fibrosis processes in different tissues share similar pathological features, such as elevated levels of pro-inflammatory factors and increased collagen fibers. In the pathogenesis of pulmonary fibrosis, the cellular senescence induced by telomere dysfunction or DNA damage plays a key role. It remains unclear whether TFL has similar therapeutic effects on lung fibrosis or aging.

To verify the anti-aging and anti-fibrotic effects of TFL *in vivo*, we used a BLM-induced pulmonary senescence and fibrosis mouse model. BLM is a commonly used chemotherapeutic drug that often causes lung injury. Its core mechanism of inducing cellular senescence involves the inhibition of DNA topoisomerase II, leading to DNA damage and subsequent genomic instability [48]. BLM-induced premature aging significantly upregulates key senescence markers, such as p21 and SA-β-Gal, as well as pro-inflammatory cytokines, including IL-1α, IL-1β, and IL-6 [49,50]. In this study, TFL was found to effectively reduce the expression of pro-inflammatory cytokines such as IL-1α and IL-1β in the lung tissue of BLM-treated mice. Moreover, TFL improved the degree of lung tissue aging and decreased the protein level of p21. H&E staining results further demonstrated that after TFL treatment, the extent of lung injury in the mice was significantly reduced. Masson’s trichrome staining revealed that TFL intervention markedly improved BLM-induced pulmonary fibrosis in mice, which is consistent with previous findings in schistosome-infected liver tissues.

To further understand the anti-aging mechanism of TFL, we

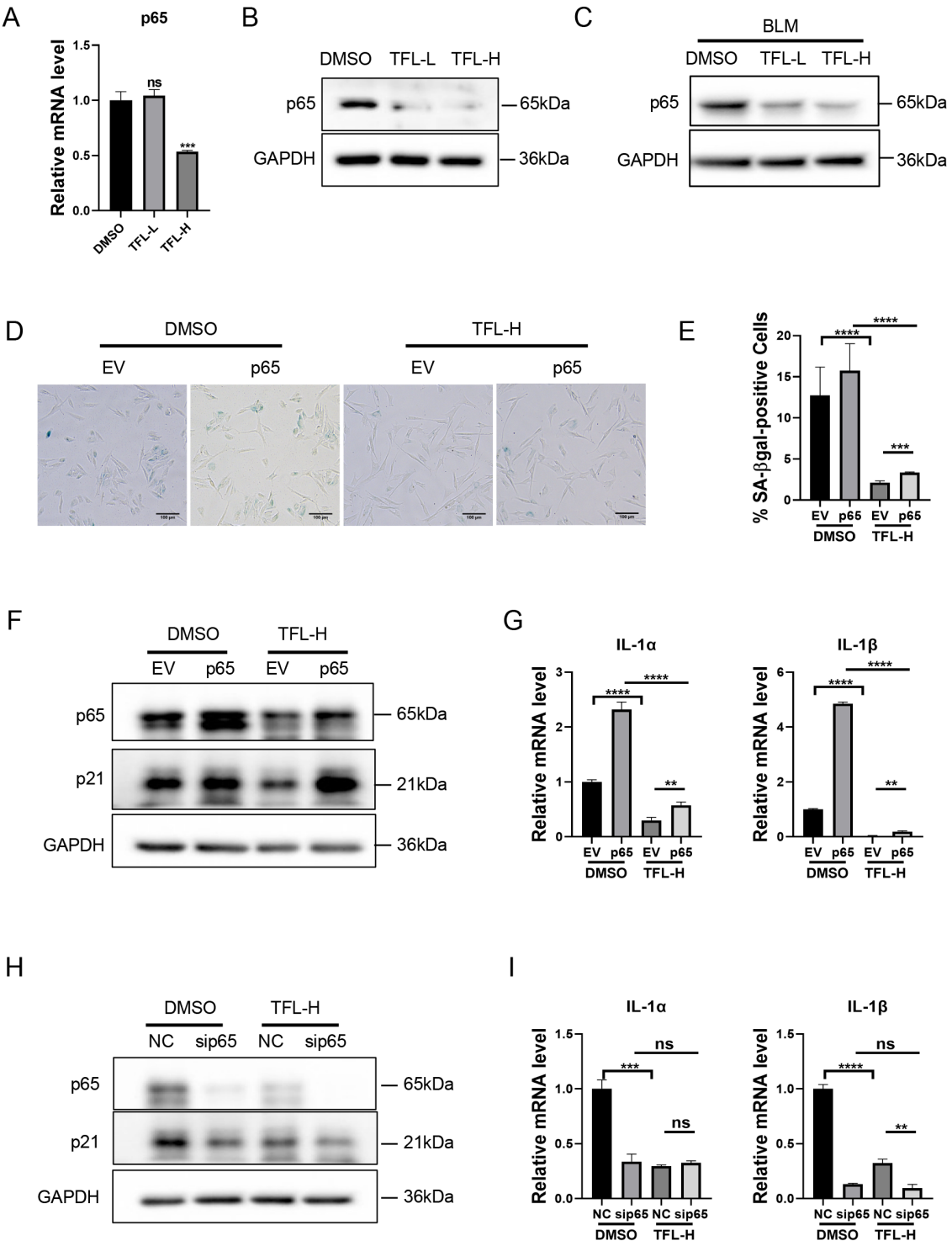

Figure 7. TFL decreases the protein level of p65 to delay cellular senescence (A) mRNA levels of the NF-κB subunit p65. RT-qPCR of PD35 MRC-5 cells treated with 300 mg/L (TFL-L) or 450 mg/L (TFL-H) TFL for 6 d. (B) Protein levels of p65 after 6 d of 300 mg/L (TFL-L) or 450 mg/L (TFL-H) TFL treatment. (C) Protein levels of p65 after 6 d of TFL treatment in BLM-induced senescence. (D) SA-β-Gal staining of PD35 MRC-5 cells transfected with EV (empty vector) or p65 plasmid and treated with 450 mg/L (TFL-H) TFL for 3 d at the same time. Scale bar: 100 μm. (E) Percentage of SA-β-Gal-positive cells from (D) ($n \geq 100$ cells). (F) The protein levels of p65 and p21 in MRC-5 cells from (D) were detected by western blotting. (G) The mRNA levels of *IL-1α* and *IL-1β* in (D) were detected by RT-qPCR. (H) Western blot analysis of p65 and p21 protein levels in PD35 MRC-5 cells transfected with NC (negative control) or si-p65 and treated with 450 mg/L TFL for 3 d at the same time. (I) mRNA levels of *IL-1α* and *IL-1β* in (H) were detected by RT-qPCR. Data are presented as the mean ± SEM. Statistical significance was assessed via two-tailed unpaired Student's *t* tests (**$P < 0.01$, ***$P < 0.001$, ****$P < 0.0001$). See also Supplementary Figure S5.

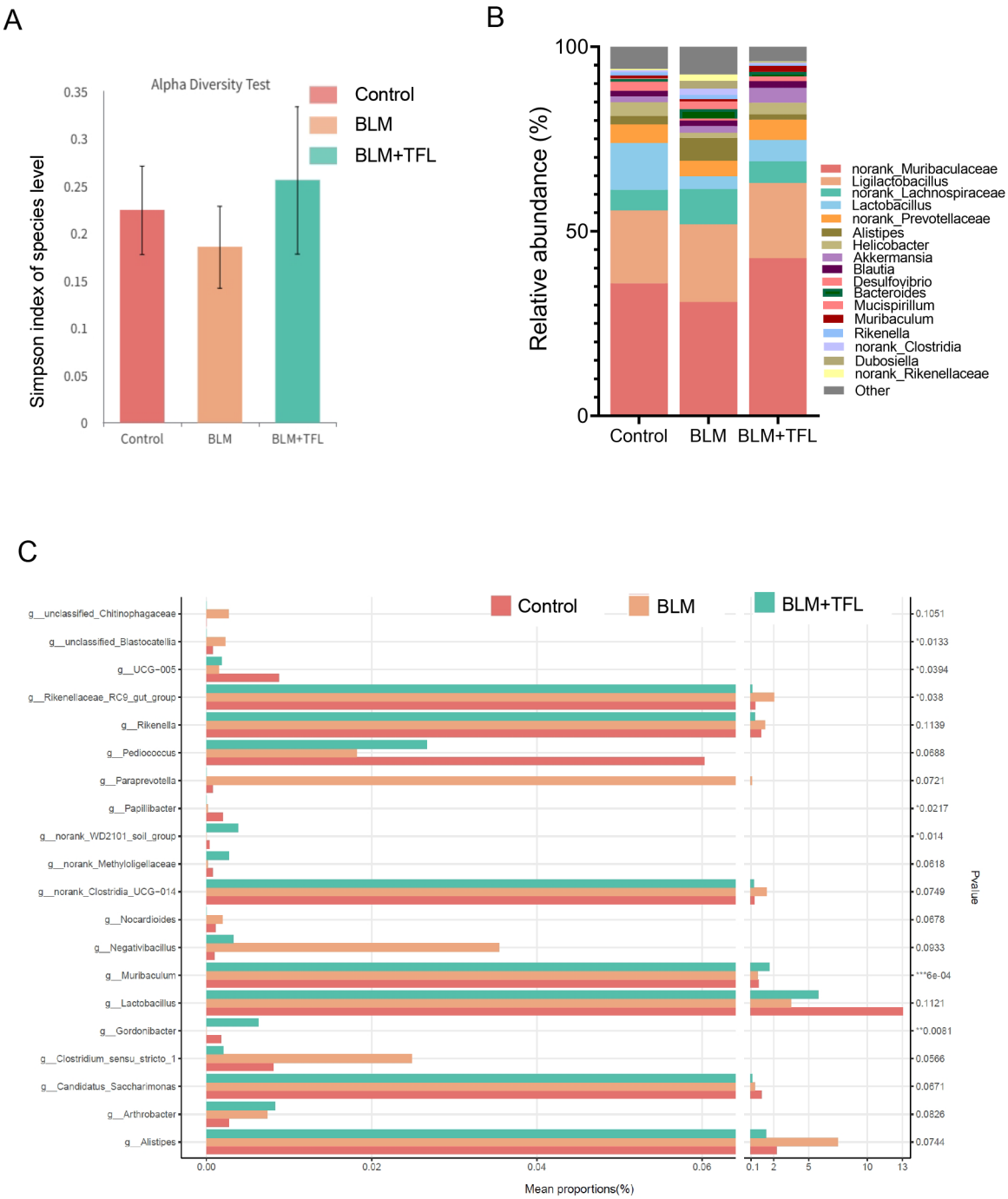

Figure 8. BLM-induced alterations in the gut microbiota are ameliorated by TFL treatment (A) Simpson index at the species level. (B) Comparison of the average relative abundances of specific gut bacteria in the control, BLM and BLM + TFL groups at the genus level. (C) Multigroup difference analysis of the 20 most abundant genera via ANOVA.

conducted RNA sequencing analysis, which showed that the NF-κB signaling pathway and metabolic pathways play important roles in its anti-aging activity. We subsequently performed gut microbiome analysis and found that TFL treatment improved the microflora changes caused by BLM treatment, which was consistent with the RNA sequencing results. We further validated the predicted anti-aging mechanisms of TFL through aging-related experiments. This study provides the first evidence that TFL improves lung fibrosis and aging in mice, thereby filling a critical research gap. These findings demonstrate the anti-fibrotic and anti-aging protective effects of TFL in a realistic disease model and its potential clinical value.

p65 is a key subunit of the NF-κB pathway that regulates cellular senescence by modulating the release of SASP factors, including IL-1α and IL-1β [51]. Downregulation of p65 is a shared phenotype among most anti-aging interventions [52]. In this study, p65 in

human lung fibroblasts was identified as a target of TFL, which is consistent with previous reports in cancer cells [53,54]. The absence of p65 can reduce the production of SASP factors, including IL-1α and IL-1β [55–57]. We downregulated p65 protein levels and simultaneously treated the cells with TFL; however, *p65* knockdown combined with TFL did not further reduce IL-1α or IL-1β expression in the *p65* knockdown group, the TFL group, or the *p65* knockdown combined with TFL group. These findings suggested that TFL improved cellular senescence through p65 in the NF-κB signaling pathway. Moreover, p65 overexpression reversed the TFL-induced reduction in IL-1α and IL-1β levels, confirming that p65 is a TFL target. Overexpression of p65 increased the mRNA levels of *IL-1α* and *IL-1β* and promoted cellular senescence, which was consistent with previous reports [42]. We did not observe a significant change in p65 protein levels in lung tissues from the BLM group or the TFL group (Supplementary Figure S3B), indicating that p65 might not be a major target in BLM-induced pulmonary fibrosis or the aging mouse model.

As mentioned earlier, TFL may improve aging phenotypes through metabolic pathways. Therefore, we conducted a gut microbiome analysis. Increasing evidence suggests that the gut microbiome is related to the occurrence and development of IPF [58,59]. On the basis of the regulatory function of the lung-gut axis, dysbiosis of the gut microbiota not only triggers immune responses regulated by the gastrointestinal tract but also affects the pathogenesis of IPF in multiple ways [60,61]. Changes in the microbiome play important roles in regulating inflammation and the activation or differentiation of fibroblasts, thereby modulating extracellular matrix formation [62]. However, the relationship between IPF and the gut microbiome is still in the exploratory stage. We compared the gut microbiota among the control group, BLM group, and BLM + TFL-H group, revealing changes that support a connection between the lung-gut axis and pulmonary fibrosis. The abundance of *Lactobacillus* is one of the most significant variations. *Lactobacillus* is a commonly-used probiotic that helps maintain the stability of the gut microecology, but it was found to decline during viral infections and inflammatory responses [63,64]. In healthy mice, the abundance of *Lactobacillus* is very high. After BLM treatment, its abundance was reduced, suggesting that a decrease in *Lactobacillus* abundance may exacerbate pulmonary fibrosis by affecting the lung-gut axis. Following TFL treatment, its abundance recovered to a relatively high level. Consistent with the report by Ruan *et al.* [59], the natural product 20(S)-protopanaxadiol can ameliorate pulmonary fibrosis progression by modulating the gut microbiota.

The antimicrobial activity of flavonoids has been widely studied. *Lactobacillus* decreases during inflammation [65], and flavonoids can restore the growth and colonization of beneficial gut bacteria such as *Lactobacillus* by inhibiting the release of inflammatory factors, thereby reducing the amount of bacterial endotoxins that trigger inflammation. This may be one of the multiple mechanisms by which TFL alleviates pulmonary fibrosis and aging. One of the factors leading to aging is microbial imbalance. We found that the microbiome in the BLM group of mice was dysregulated, and after TFL treatment, the microbiota distribution was restored to levels close to those of the control group, indicating that TFL can improve the gut microbiome, which may also be another mechanism by which TFL alleviates pulmonary fibrosis and aging. However, whether the lung-gut connection is driven by changes in the intestinal barrier, leakage of gut microbial metabolites affecting IPF, or immune responses generated by IPF linking the lung and gut still remains to be explored in depth.

In recent years, increasing attention has focused on identifying effective and low-toxicity natural compounds to combat IPF. Existing evidence suggests that quercetin is most likely to be used in combination with other therapeutic agents. Studies have shown that active ingredients in single herbs and traditional Chinese medicine formulas, especially flavonoids, have potential therapeutic effects on pulmonary fibrosis. The underlying mechanisms may involve the modulation of inflammatory responses and pro-fibrotic signaling pathways [66]. As a flavonoid compound with anti-inflammatory, anti-aging, and anti-fibrotic therapeutic effects, the core components of TFL include rutin, quercetin, morin, *etc.* [35,37]. Both quercetin monomers and rutin monomers have been proven to scavenge free radicals, thereby delaying aging. The most common current method of administration involves combining quercetin with other drugs.

Previous studies have indicated that the combination of quercetin and dasatinib significantly improved pulmonary fibrosis by reducing the SASP or clearing senescent cells [12,67,68]. Quercetin can alleviate silica-induced pulmonary fibrosis by inhibiting macrophage senescence [69]. It also inhibits alveolar epithelial cell senescence [70], and when combined with 3′,5′-dimaleimide benzoic acid, it can reduce lung fibrosis in systemic sclerosis models [71]. Quercetin-3-rutinoside mitigates radiation-induced pulmonary inflammation and fibrosis by modulating the NF-κB/TGF-β1 signaling pathway [72]. Therefore, the improvement in pulmonary fibrosis and delay of aging by TFL may be due to the synergistic effects of active ingredients such as quercetin and rutin.

In summary, we demonstrate that TFL delays cellular senescence by suppressing the protein level of p65, thereby reducing SASP secretion. Furthermore, TFL alleviates pulmonary fibrosis and senescence by enriching the beneficial gut microbiota via the gut-lung axis. These findings highlight TFL's potential as an anti-aging therapeutic agent.

Supplementary Data

Supplementary data are available at *Acta Biochimica et Biophysica Sinica* online.

Data Availability

The transcriptomics data generated in this study have been deposited in the Genome Sequence Archive in National Genomics Data Center, China National Center for Bioinformation, Chinese Academy of Sciences (accession number: HRA014172) that are publicly accessible at https://ngdc.cncb.ac.cn/gsa-human.

Funding

This work was supported by the grants from the National Natural Science Foundation of China (No. 32200604), the Natural Science Foundation of Guangxi (No. 2023GXNSFBA026015), the First-class Discipline Innovation-driven Talent Program of Guangxi Medical University to Xiaocui Li and Tingzheng Zhan, and a Research Grant of Key Laboratory of Regenerative Medicine of Ministry of Education, Jinan University (No. ZSYXQ202504).

Conflict of Interest

The authors declare that they have no conflict of interest.

References

1. de Magalhães JP. How ageing processes influence cancer. *Nat Rev Cancer* 2013, 13: 357–365
2. North BJ, Sinclair DA. The intersection between aging and cardiovascular disease. *Circ Res* 2012, 110: 1097–1108
3. Cai Y, Song W, Li J, Jing Y, Liang C, Zhang L, Zhang X, *et al.* The landscape of aging. *Sci China Life Sci* 2022, 65: 2354–2454
4. Nalysnyk L, Cid-Ruzafa J, Rotella P, Esser D. Incidence and prevalence of idiopathic pulmonary fibrosis: review of the literature. *Eur Respir Rev* 2012, 21: 355–361
5. Gunasekaran U, Gannon M. Type 2 diabetes and the aging pancreatic beta cell. *Aging* 2011, 3: 565–575
6. Huang Y, Peng H, Wu Y, Deng S, Ge F, Ma W, Zhou X, *et al.* Rosa roxburghii fruit extracts upregulate telomerase activity and ameliorate cell replicative senescence. *Foods* 2024, 13: 1673
7. Hernandez-Segura A, Nehme J, Demaria M. Hallmarks of cellular senescence. *Trends Cell Biol* 2018, 28: 436–453
8. Wang B, Han J, Elisseeff JH, Demaria M. The senescence-associated secretory phenotype and its physiological and pathological implications. *Nat Rev Mol Cell Biol* 2024, 25: 958–978
9. Campisi J, d'Adda di Fagagna F. Cellular senescence: when bad things happen to good cells. *Nat Rev Mol Cell Biol* 2007, 8: 729–740
10. López-Otín C, Blasco MA, Partridge L, Serrano M, Kroemer G. Hallmarks of aging: an expanding universe. *Cell* 2023, 186: 243–278
11. Kroemer G, Maier AB, Cuervo AM, Gladyshev VN, Ferrucci L, Gorbunova V, Kennedy BK, *et al.* From geroscience to precision geromedicine: understanding and managing aging. *Cell* 2025, 188: 2043–2062
12. Schafer MJ, White TA, Iijima K, Haak AJ, Ligresti G, Atkinson EJ, Oberg AL, *et al.* Cellular senescence mediates fibrotic pulmonary disease. *Nat Commun* 2017, 8: 14532
13. Richeldi L, Collard HR, Jones MG. Idiopathic pulmonary fibrosis. *Lancet* 2017, 389: 1941–1952
14. Wuyts WA, Agostini C, Antoniou KM, Bouros D, Chambers RC, Cottin V, Egan JJ, *et al.* The pathogenesis of pulmonary fibrosis: a moving target. *Eur Respir J* 2013, 41: 1207–1218
15. Wynn TA. Integrating mechanisms of pulmonary fibrosis. *J Exp Med* 2011, 208: 1339–1350
16. Alder JK, Barkauskas CE, Limjunyawong N, Stanley SE, Kembou F, Tuder RM, Hogan BLM, *et al.* Telomere dysfunction causes alveolar stem cell failure. *Proc Natl Acad Sci USA* 2015, 112: 5099–5104
17. Armanios MY, Chen JJL, Cogan JD, Alder JK, Ingersoll RG, Markin C, Lawson WE, *et al.* Telomerase mutations in families with idiopathic pulmonary fibrosis. *N Engl J Med* 2007, 356: 1317–1326
18. Gasse P, Mary C, Guenon I, Noulin N, Charron S, Schnyder-Candrian S, Schnyder B, *et al.* IL-1R1/MyD88 signaling and the inflammasome are essential in pulmonary inflammation and fibrosis in mice. *J Clin Invest* 2007, 117: 3786–3799
19. Suwara MI, Green NJ, Borthwick LA, Mann J, Mayer-Barber KD, Barron L, Corris PA, *et al.* IL-1α released from damaged epithelial cells is sufficient and essential to trigger inflammatory responses in human lung fibroblasts. *Mucosal Immunol* 2014, 7: 684–693
20. Hickson LTJ, Langhi Prata LGP, Bobart SA, Evans TK, Giorgadze N, Hashmi SK, Herrmann SM, *et al.* Senolytics decrease senescent cells in humans: preliminary report from a clinical trial of dasatinib plus quercetin in individuals with diabetic kidney disease. *EBioMedicine* 2019, 47: 446–456
21. Jaskelioff M, Muller FL, Paik JH, Thomas E, Jiang S, Adams AC, Sahin E, *et al.* Telomerase reactivation reverses tissue degeneration in aged telomerase-deficient mice. *Nature* 2010, 469: 102–106
22. Dong Z, Luo Y, Yuan Z, Tian Y, Jin T, Xu F. Cellular senescence and SASP in tumor progression and therapeutic opportunities. *Mol Cancer* 2024, 23: 181
23. Anighoro A, Bajorath J, Rastelli G. Polypharmacology: challenges and opportunities in drug discovery. *J Med Chem* 2014, 57: 7874–7887
24. Yıldırım MA, Goh KI, Cusick ME, Barabási AL, Vidal M. Drug—target network. *Nat Biotechnol* 2007, 25: 1119–1126
25. Wang J, Liu W, Huang Y, Wang G, Guo X, Shi D, Sun T, *et al.* A senomorphlytic three-drug combination discovered in *salsola collina* for delaying aging phenotypes and extending healthspan. *Adv Sci* 2024, 11: e2401862
26. Jen Cl, Su CH, Lu MK, Lai MM, Ng LT. Synergistic anti-inflammatory effects of different polysaccharide components from *Xylaria nigripes*. *J Food Biochem* 2021, 45: e13694
27. Zhou X, Seto SW, Chang D, Kiat H, Razmovski-Naumovski V, Chan K, Bensoussan A. Synergistic effects of chinese herbal medicine: a comprehensive review of methodology and current research. *Front Pharmacol* 2016, 7: 201
28. Phu HT, Thuan DTB, Nguyen THD, Posadino AM, Eid AH, Pintus G. Herbal medicine for slowing aging and aging-associated conditions: efficacy, mechanisms and safety. *CVP* 2020, 18: 369–393
29. Cheng F, Kovács IA, Barabási AL. Publisher correction: network-based prediction of drug combinations. *Nat Commun* 2019, 10: 1806
30. Shen C-, Jiang J-, Yang L, Wang D-, Zhu W. Anti-ageing active ingredients from herbs and nutraceuticals used in traditional Chinese medicine: pharmacological mechanisms and implications for drug discovery. *Br J Pharmacol* 2016, 174: 1395–1425
31. Zeng SL, Li SZ, Xiao PT, Cai YY, Chu C, Chen BZ, Li P, *et al.* Citrus polymethoxyflavones attenuate metabolic syndrome by regulating gut microbiome and amino acid metabolism. *Sci Adv* 2020, 6: eaax6208
32. Fan B, Li Y, Bi Y, Tong L, Li D, Wang Y. Design of multi-drug combinations for poly-pharmacological effects using composition-activity relationship modeling and multi-objective optimization approach: application in traditional Chinese medicine. *Chem Biol Drug Des* 2018, 93: 1073–1082
33. Liao Y, Luo Z, Liu Y, Xue W, He S, Chen X, Ren H, *et al.* Total flavonoids of Litchi seed attenuate stem cell-like properties in breast cancer by regulating Notch3 signaling pathway. *J EthnoPharmacol* 2023, 305: 116133
34. Yang X, Liu S, Liu Y, Wang Y, Cui D, Lan T, Zhu D, *et al.* Total flavonoids of litchi seed inhibit breast cancer metastasis by regulating the PI3K/AKT/mTOR and MAPKs signaling pathways. *Pharm Biol* 2025, 63: 229–249
35. Li Q, Wang J, Lv J, Liu D, Xiao S, Mo J, Lu Z, *et al.* Total flavonoids of litchi Seed alleviates schistosomiasis liver fibrosis in mice by suppressing hepatic stellate cells activation and modulating the gut microbiomes. *Biomed Pharmacother* 2024, 178: 117240
36. Yan J, Feng Y, Fang X, Cui X, Xia X, Li F, Luo W, *et al.* Anti-liver fibrosis effects of the total flavonoids of litchi semen on CCl_4-induced liver fibrosis in rats associated with the upregulation of retinol metabolism. *Pharm Biol* 2022, 60: 1264–1277
37. Luo L, Wang J, Cheng Q, Lu Z, Lv J, Xiao S, Tang L, *et al.* Investigation of the inhibitory effects of total flavonoids of litchi seed on clonorchis sinensis-induced liver damage and fibrosis. *Front Cell Infect Microbiol* 2025, 15: 1625004
38. Hübner RH, Gitter W, Eddine El Mokhtari N, Mathiak M, Both M, Bolte H, Freitag-Wolf S, *et al.* Standardized quantification of pulmonary fibrosis in histological samples. *BioTechniques* 2008, 44: 507–517
39. Wan R, Wang L, Zhu M, Li W, Duan Y, Yu G. Cellular senescence: a troy horse in pulmonary fibrosis. *Int J Mol Sci* 2023, 24: 16410

40. Liu T, De Los Santos FG, Phan SH. The bleomycin model of pulmonary fibrosis. *Methods Mol Biol* 2017, 1627: 27–42
41. Mato-Basalo R, Morente-López M, Arntz OJ, van de Loo FAJ, Fafián-Labora J, Arufe MC. Therapeutic potential for regulation of the nuclear factor Kappa-B transcription factor p65 to prevent cellular senescence and activation of pro-inflammatory in mesenchymal stem cells. *Int J Mol Sci* 2021, 22: 3367
42. Chien Y, Scuoppo C, Wang X, Fang X, Balgley B, Bolden JE, Premsrirut P, ***et al.*** Control of the senescence-associated secretory phenotype by NF-κB promotes senescence and enhances chemosensitivity. *Genes Dev* 2011, 25: 2125–2136
43. Shao J, Li Z, Gao Y, Zhao K, Lin M, Li Y, Wang S, ***et al.*** Construction of a "bacteria-metabolites" co-expression network to clarify the anti–ulcerative colitis effect of flavonoids of sophora flavescens aiton by regulating the "host–microbe" interaction. *Front Pharmacol* 2021, 12: 710052
44. Zhu Y, Chen B, Zhang X, Akbar MT, Wu T, Zhang Y, Zhi L, ***et al.*** Exploration of the muribaculaceae family in the gut microbiota: diversity, metabolism, and function. *Nutrients* 2024, 16: 2660
45. Wang Z, Dan W, Zhang N, Fang J, Yang Y. Colorectal cancer and gut microbiota studies in China. *Gut Microbes* 2023, 15: 2236364
46. Feng Q, Liang S, Jia H, Stadlmayr A, Tang L, Lan Z, Zhang D, ***et al.*** Gut microbiome development along the colorectal adenoma-carcinoma sequence. *Nat Commun* 2015, 6: 6528
47. Wan D, Qin D, Tian J, L. X, Liu J, Zhang H. Preparation of litchi nut extract and acute toxicity test. *Journal of Luzhou Medical College* 2010, 33: 28–30
48. Hay J, Shahzeidi S, Laurent G. Mechanisms of bleomycin-induced lung damage. *Arch Toxicol* 1991, 65: 81–94
49. Zhang C, Chen L, Xie C, Wang F, Wang J, Zhou H, Liu Q, ***et al.*** YTHDC1 delays cellular senescence and pulmonary fibrosis by activating ATR in an m6A-independent manner. *EMBO J* 2023, 43: 61–86
50. Zhou H, Xie C, Xie Y, He Y, Chen Y, Zhang C, Zhang Y, ***et al.*** UBQLN1 deficiency mediates telomere shortening and IPF through interacting with RPA1. *PLoS Genet* 2023, 19: e1010856
51. Salminen A, Kauppinen A, Kaarniranta K. Emerging role of NF-κB signaling in the induction of senescence-associated secretory phenotype (SASP). *Cell Signal* 2012, 24: 835–845
52. Elmansi AM, Kassem A, Castilla RM, Miller RA. Downregulation of the NF-κB protein p65 is a shared phenotype among most anti-aging interventions. *GeroScience* 2024, 47: 3077–3094
53. Zhang W, Chen T, Yang P, Li X, Zhu D, Su Z, Yang X, ***et al.*** Total flavonoids of Litchi chinensis Sonn. seed inhibit prostate cancer growth in bone by regulating the bone microenvironment via inactivation of the HGFR/NF-κB signaling pathway. *J EthnoPharmacol* 2024, 319: 117327
54. Chang M, Zhu D, Chen Y, Zhang W, Liu X, Li XL, Cheng Z, ***et al.*** Total flavonoids of litchi seed attenuate prostate cancer progression via inhibiting AKT/mTOR and NF-kB signaling pathways. *Front Pharmacol* 2021, 12: 758219
55. Lee UJ, Choung SR, Prakash KVB, Lee EJ, Lee MY, Kim YJ, Han CW, ***et al.*** Dual knockdown of p65 and p50 subunits of NF-kappaB by siRNA inhibits the induction of inflammatory cytokines and significantly enhance apoptosis in human primary synoviocytes treated with tumor necrosis factor-alpha. *Mol Biol Rep* 2007, 35: 291–298
56. Singh AK, Fechtner S, Chourasia M, Sicalo J, Ahmed S. Critical role of IL-1α in IL-1β-induced inflammatory responses: cooperation with NF-κBp65 in transcriptional regulation. *FASEB Journal* 2019, 33: 2526–2536
57. Liu T, Zhang L, Joo D, Sun SC. NF-κB signaling in inflammation. *Sig Transduct Target Ther* 2017, 2: 17023
58. Dong Y, He L, Zhu Z, Yang F, Ma Q, Zhang Y, Zhang X, ***et al.*** The mechanism of gut-lung axis in pulmonary fibrosis. *Front Cell Infect Microbiol* 2024, 14: 1258246
59. Ruan Y, Ren G, Wang M, Lv W, Shimizu K, Zhang C. The dual role of 20 (S)-protopanaxadiol in alleviating pulmonary fibrosis through the gut-lung axis. *Phytomedicine* 2024, 129: 155699
60. Yoon Y, Hrusch CL, Fei N, Barrón GM, Mills KAM, Hollinger MK, Velez TE, ***et al.*** Gut microbiota modulates bleomycin-induced acute lung injury response in mice. *Respir Res* 2022, 23: 337
61. Wypych TP, Wickramasinghe LC, Marsland BJ. The influence of the microbiome on respiratory health. *Nat Immunol* 2019, 20: 1279–1290
62. Zhan S, Li N, Liu C, Mao R, Wu D, Li T, Chen M, ***et al.*** Intestinal fibrosis and gut microbiota: clues from other organs. *Front Microbiol* 2021, 12: 694967
63. Wang Y, Wu Y, Wang Y, Xu H, Mei X, Yu D, Wang Y, ***et al.*** Antioxidant properties of probiotic bacteria. *Nutrients* 2017, 9: 521
64. Li Z, Shen Y, Xin J, Xu X, Ding Q, Chen W, Wang J, ***et al.*** Cryptotanshinone alleviates radiation-induced lung fibrosis via modulation of gut microbiota and bile acid metabolism. *PhytoTher Res* 2023, 37: 4557–4571
65. Kostic AD, Xavier RJ, Gevers D. The microbiome in inflammatory bowel disease: current status and the future ahead. *Gastroenterology* 2014, 146: 1489–1499
66. Li LC, Kan LD. Traditional Chinese medicine for pulmonary fibrosis therapy: progress and future prospects. *J EthnoPharmacol* 2017, 198: 45–63
67. Justice JN, Nambiar AM, Tchkonia T, LeBrasseur NK, Pascual R, Hashmi SK, Prata L, ***et al.*** Senolytics in idiopathic pulmonary fibrosis: results from a first-in-human, open-label, pilot study. *EBioMedicine* 2019, 40: 554–563
68. Kirkland JL, Tchkonia T. Senolytic drugs: from discovery to translation. *J Intern Med* 2020, 288: 518–536
69. Geng F, Xu M, Zhao L, Zhang H, Li J, Jin F, Li Y, ***et al.*** Quercetin alleviates pulmonary fibrosis in mice exposed to silica by inhibiting macrophage senescence. *Front Pharmacol* 2022, 13: 912029
70. Wu W, Wu X, Qiu L, Wan R, Zhu X, Chen S, Yang X, ***et al.*** Quercetin influences intestinal dysbacteriosis and delays alveolar epithelial cell senescence by regulating PTEN/PI3K/AKT signaling in pulmonary fibrosis. *Naunyn Schmiedebergs Arch Pharmacol* 2023, 397: 4809–4822
71. Reyes-Jiménez E, Ramírez-Hernández AA, Santos-Álvarez JC, Velázquez-Enríquez JM, González-García K, Carrasco-Torres G, Villa-Treviño S, ***et al.*** Coadministration of 3′5-dimaleamylbenzoic acid and quercetin decrease pulmonary fibrosis in a systemic sclerosis model. *Int Immunopharmacol* 2023, 122: 110664
72. Verma S, Dutta A, Dahiya A, Kalra N. Quercetin-3-Rutinoside alleviates radiation-induced lung inflammation and fibrosis via regulation of NF-κB/TGF-β1 signaling. *Phytomedicine* 2022, 99: 154004